

# Variational Phase Estimation with Variational Fast Forwarding

Maria-Andreea Filip, David Muñoz Ramo, and Nathan Fitzpatrick\*

*Quantinuum  
13-15 Hills Road, CB2 1NL,  
Cambridge, United Kingdom*

(Dated: November 30, 2022)

Subspace diagonalisation methods have appeared recently as promising means to access the ground state and some excited states of molecular Hamiltonians by classically diagonalising small matrices, whose elements can be efficiently obtained by a quantum computer. The recently proposed Variational Quantum Phase Estimation (VQPE) algorithm uses a basis of real time-evolved states, for which the energy eigenvalues can be obtained directly from the unitary matrix  $\mathbf{U} = e^{-i\mathbf{H}\Delta t}$ , which can be computed with cost linear in the number of states used. In this paper, we report a circuit-based implementation of VQPE for arbitrary molecular systems and assess its performance and costs for the  $\text{H}_2$ ,  $\text{H}_3^+$  and  $\text{H}_6$  molecules. We also propose using Variational Fast Forwarding (VFF) to decrease to quantum depth of time-evolution circuits for use in VQPE. We show that the approximation provides a good basis for Hamiltonian diagonalisation even when its fidelity to the true time evolved states is low. In the high fidelity case, we show that the approximate unitary  $\mathbf{U}$  can be diagonalised instead, preserving the linear cost of exact VQPE.

## I. INTRODUCTION

The current era of noisy intermediate scale quantum (NISQ) devices[1] is dominated by hybrid quantum-classical algorithms like the variational quantum eigensolver (VQE).[2] In this approach a cost function is calculated on a quantum computer and then minimized using a classical optimization procedure, with the aim of reducing the amount of quantum computation to a level manageable on current architectures, built of noisy gates and qubits with low coherence times. VQE has found use in quantum chemistry applications,[3, 4] where the goal often is finding estimates of the lowest eigenvalue(s) of the molecular Hamiltonian. Alternative hybrid approaches to this problem have also been developed, based on the imaginary-time evolution of the system[5] and, more recently, on real-time evolution.[6]

Quantum Phase Estimation (QPE)[7] — which uses the repeated application of a unitary and the quantum Fourier transform to estimate the phase of the unitary — was one of the first quantum algorithms highlighted for quantum chemistry, by using it on the real-time evolution operator to get the lowest eigenvalue of the Hamiltonian.[8] However, its quantum resource requirements make it intractable on NISQ devices. The recently developed Variational Quantum Phase Estimation (VQPE) algorithm[9] uses time evolved states as a basis for non-orthogonal configuration interaction (NOCI). The NOCI matrix elements are computed on the quantum processor, while the diagonalisation is carried out classically. It has been shown that only relatively few states and a linear number of measurements

are needed.

This algorithm is part of a wider class of quantum subspace diagonalisation (QSD) methods,[6, 10–14] in which non-orthogonal states are used as a basis to solve the generalised Hamiltonian eigenvalue problem, giving estimates for multiple eigenstates. Many of these methods, including VQPE, perform the diagonalisation in a Krylov subspace[15] obtained by the repeated application of some unitary.[13, 14]

In this paper, we describe a quantum circuit based implementation of the VQPE algorithm for general molecular Hamiltonians and assess the hardware requirements of such a method. We also investigate using Variational Fast Forwarding (VFF)[16, 17] to approximate time-evolution and the effects this approximation has on the resulting non-orthogonal CI calculation.

We begin with an overview of the VQE, QPE and VQPE algorithms. Sec. III gives VQPE results for a range of small molecules and the Hubbard model, while Section IV gives results for VQPE based on the VFF approximation. Conclusions are drawn in Sec. V.

## II. QUANTUM ALGORITHMS

### A. Quantum Phase Estimation

Given a unitary operator  $\hat{U}$  and one of its eigenfunctions  $|\Psi\rangle$  such that  $\hat{U}|\Psi\rangle = e^{i2\pi\theta}|\Psi\rangle$ , QPE can be used to estimate the value of  $\theta$ .

For a hermitian Hamiltonian  $\hat{H}$ , the corresponding time-evolution operator  $\hat{U} = e^{-i\hat{H}t}$  is unitary and may be used in QPE, using the circuit given in Fig. 1. Before the inverse quantum Fourier transform (QFT), the

\* [nathan.fitzpatrick@quantinuum.com](mailto:nathan.fitzpatrick@quantinuum.com)

generated wavefunction is given by

$$|\Psi_{\text{QPE}}\rangle = \frac{1}{2^{n/2}} \sum_{j=0}^{2^n-1} e^{-i\hat{H}tj} |j\rangle |\psi\rangle. \quad (1)$$

where  $|j\rangle$  is the qubit product state corresponding to the binary encoding of  $j$ . Taking the inverse quantum Fourier transform gives

$$\text{QFT}^{-1}[|\Psi_{\text{QPE}}\rangle] = \frac{1}{2^{n/2}} \sum_{k=0}^{2^n-1} |k\rangle \left( \sum_{j=0}^{2^n-1} e^{-itj(\omega_k + \hat{H})} |\psi\rangle \right), \quad (2)$$

where  $\omega_k = 2\pi k/(2^n t)$ . If  $|\psi\rangle$  is an eigenfunction of  $\hat{H}$ ,

$$\hat{H} |\psi\rangle = E |\psi\rangle, \quad (3)$$

this reduces to

$$\text{QFT}^{-1}[|\Psi_{\text{QPE}}\rangle] = \frac{1}{2^{n/2}} \sum_{k=0}^{2^n-1} |k\rangle \left( \sum_{j=0}^{2^n-1} e^{-itj(\omega_k + E)} |\psi\rangle \right), \quad (4)$$

which peaks around  $\omega_k = -E$ , so measurement is highly likely to give an  $n$ -bit integer approximation of  $k = -2^n t E / 2\pi$ .

Provided a guess wavefunction  $|\tilde{\psi}\rangle$ , QPE will successfully generate the eigenvalue  $E$  with probability proportional to  $|\langle \tilde{\psi} | \psi \rangle|^2$ .<sup>[8]</sup> As such, if one has access to a wavefunction with good overlap with the ground state of a quantum system, QPE can be used to estimate the true ground state energy with high probability. For quantum chemical systems, the Hartree–Fock (HF) wavefunction may often be good enough, but techniques such as adiabatic state preparation<sup>[18, 19]</sup> may be used to improve upon it.

## B. Variational Quantum Phase Estimation

Like the standard phase estimation algorithm, Variational Phase Estimation (VQPE) requires a reference state with some non-zero overlap with the eigenbasis of the Hamiltonian. We can expand the reference state  $|\Phi_0\rangle$  in terms of the eigenfunctions  $|N\rangle$  as

$$|\Phi_0\rangle = \sum_N \phi_N^0 |N\rangle, \quad (5)$$

where  $\phi_N^0 = \langle N | \Phi_0 \rangle$ . The key step in VQPE is to define a series of time-evolved states  $|\Phi_{j,0}\rangle$ ,

$$|\Phi_{j,0}\rangle = e^{-i\hat{H}tj} |\Phi_0\rangle, \quad (6)$$

which can also be expanded in the eigenbasis of  $\hat{H}$  as

$$|\Phi_{j,0}\rangle = \sum_N^Q \phi_N^0 e^{-iE_N t j} |N\rangle. \quad (7)$$

These time-evolved states form a Krylov subspace which may be used as a basis for configuration interaction (CI) or exact diagonalisation (ED) [20]. Consider a wavefunction

$$|\Psi\rangle = \sum_{j=0}^{N_T} c_j |\Phi_{j,0}\rangle. \quad (8)$$

Minimising  $\langle E \rangle$  with respect to all  $c_j$  for this wavefunction according to the variational principle is equivalent to solving the generalized eigenvalue problem

$$\mathbf{H}\mathbf{c} = \epsilon \mathbf{S}\mathbf{c}. \quad (9)$$

where the elements of matrices  $\mathbf{H}$  and  $\mathbf{S}$  are given by

$$H_{jk} = \langle \Phi_{j,0} | \hat{H} | \Phi_{k,0} \rangle \quad (10)$$

and

$$S_{jk} = \langle \Phi_{j,0} | \Phi_{k,0} \rangle = \langle \Phi_0 | e^{-i\hat{H}(t_k - t_j)} | \Phi_0 \rangle \quad (11)$$

respectively. Solving this matrix equation gives approximate values for  $N_T + 1$  eigenvalues of  $\hat{H}$ .

Consider the overlap operator

$$\begin{aligned} \hat{S} &= \sum_{j=0}^{N_T} |\Phi_{j,0}\rangle \langle \Phi_{j,0}| \\ &= \sum_{N,M}^Q \phi_N^0 \phi_M^{0*} \left[ \sum_{j=0}^{N_T} e^{-it_j(E_N - E_M)} \right] |N\rangle \langle M|. \end{aligned} \quad (12)$$

The original work by Klymko *et al.*[9] defines a set of phase cancellation conditions,

$$\frac{1}{N_T + 1} \sum_{j=0}^{N_T} e^{-it_j(E_N - E_M)} = \delta_{N,M} \quad (13)$$

under which

$$\hat{S} = (N_T + 1) \sum_N^Q |\phi_N^0|^2 |N\rangle \langle N|. \quad (14)$$

If these conditions are satisfied then the set of time-evolved states will span the full support space of the initial state and VQPE will be able to perfectly recover all the eigenstates in that support space. This requires at least as many time-evolved states as there are eigenstates in the support space, which may not be tractable for general systems. However, even an incomplete basis may give a good approximation for the

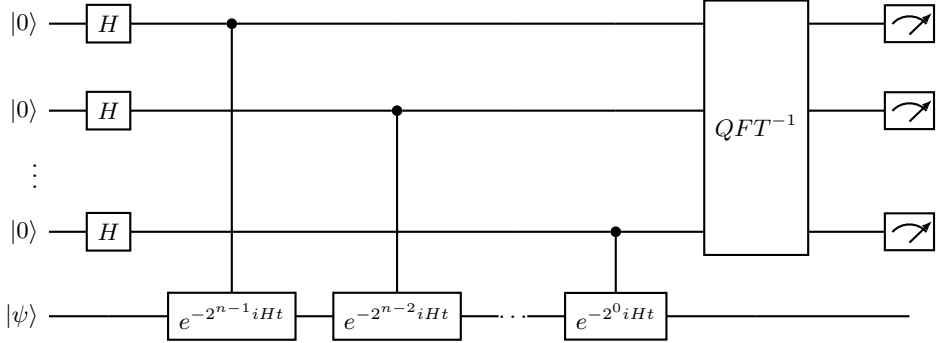


Figure 1. QPE circuit.

ground state energy of the system. Additionally, the fact that time-evolution does not introduce any additional eigenstates beyond those present in the initial states guarantees that a minimal number of basis states is needed to resolve those eigenvectors. For traditional configuration interaction algorithms like configuration interaction with single and double excitations (CISD) or NOCI, there are no such guarantees in place.

An alternative to Eq. (9) may be defined by considering the time evolution operator  $\hat{U}(\Delta t) = e^{-i\hat{H}\Delta t}$ . For eigenfunctions of the Hamiltonian,

$$\hat{U}(\Delta t) |N\rangle = e^{-iE_N\Delta t} |N\rangle. \quad (15)$$

Therefore we can define an alternate generalised eigenvalue problem,

$$\mathbf{U}(\Delta t)\mathbf{c} = \lambda \mathbf{S}\mathbf{c}. \quad (16)$$

The solutions to Eqs. (9) and (16) are related in the same way as the corresponding operators, up to a phase factor:

$$\epsilon_N = -\frac{\log(\lambda_N)}{i\Delta t} \pm \frac{2n\pi}{\Delta t}. \quad (17)$$

The time evolution matrix elements are given by

$$\begin{aligned} U_{jk} &= \langle \Phi_{j,0} | e^{-i\hat{H}\Delta t} | \Phi_{k,0} \rangle \\ &= \langle \Phi_0 | e^{-i\hat{H}(\Delta t + t_k - t_j)} | \Phi_0 \rangle \end{aligned} \quad (18)$$

In the case where a uniform time grid  $t_j = j\Delta t$  is used, these coincide with elements of the overlap matrix

$$U_{j,k} = S_{j,k+1} = S_{j-1,k}. \quad (19)$$

Therefore, while Eq. (9) requires separate measurements of all Hamiltonian and overlap matrix elements, for Eq. (16) one only needs to measure the elements of

the overlap matrix to obtain both  $\mathbf{U}$  and  $\mathbf{S}$ . Furthermore, in the uniform time grid case

$$\begin{aligned} S_{jk} &= \langle \Phi_0 | e^{-i\hat{H}(t_k - t_j)} | \Phi_0 \rangle \\ &= \langle \Phi_0 | e^{-i\hat{H}\Delta t(k-j)} | \Phi_0 \rangle \\ &= S_{j+n,k+n}, \quad \forall n \in \mathbb{Z} \end{aligned} \quad (20)$$

Therefore to construct the full overlap matrix, one only needs to compute one row of elements. This is a significant advantage to this algorithm, as it reduces the number of measurements to be linear in the number of time-evolved states rather than quadratic. As in direct Hamiltonian diagonalisation, the eigenvalues of  $\hat{U}$  provide estimates for both the ground and excited states of the system, although the presence of phase factors may confuse the identity of the states. Finding the eigenvectors of  $\hat{U}$  would then give the variationally optimised parameters  $c_j$  in Eq. (8).

### 1. Comparison to Quantum Phase Estimation

Consider  $N_T = 2^n - 1$  time-evolved states using an evenly-spaced time-grid, where  $n$  is the number of measurement qubits in the QPE circuit. The QPE wavefunction in Eq. (1) can be expressed in this basis as

$$|\Psi_{\text{QPE}}\rangle = \frac{1}{\sqrt{N_T + 1}} \sum_{j=0}^{N_T} |j\rangle |\phi_{j,0}\rangle. \quad (21)$$

Similarly, the result of the inverse QFT is given by

$$\begin{aligned} \text{QFT}^{-1}[|\Psi_{\text{QPE}}\rangle] &= \frac{1}{N_T + 1} \sum_{k=0}^{N_T} |k\rangle \left( \sum_{j=0}^{N_T} e^{i\omega_k t_j} |\phi_{j,0}\rangle \right) \\ &= \frac{1}{\sqrt{N_T + 1}} \sum_{k=0}^{N_T} |k\rangle |\omega_k\rangle. \end{aligned} \quad (22)$$

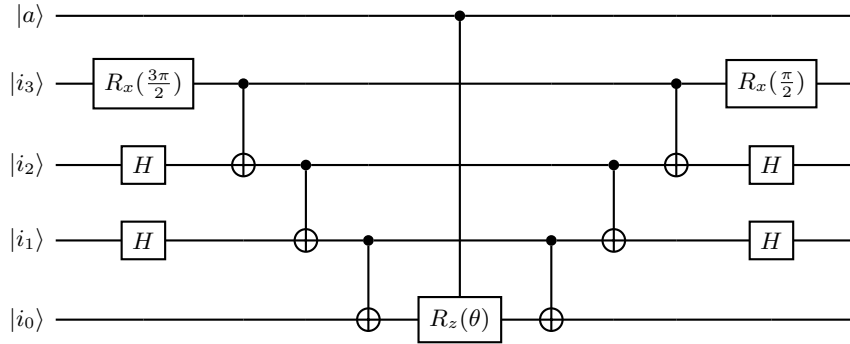


Figure 2. Controlled Pauli gadget for  $e^{-i\frac{\theta}{2}(Z_0 \otimes X_1 \otimes X_2 \otimes Y_3)}$

where

$$|\omega_k\rangle = \frac{1}{\sqrt{N_T + 1}} \sum_{j=0}^{N_T} e^{i\omega_k t_j} |\phi_{j,0}\rangle \quad (23)$$

form a Fourier basis. We can alternatively consider these as particular linear combinations of the VQPE time-evolved states,  $|\phi_{j,0}\rangle$ . In order to obtain these same states from the VQPE algorithm, the Fourier basis would need to correspond to the solutions to the corresponding VQPE generalised eigenvalue problem. In that case, the resulting VQPE energy would also correspond to the QPE estimate, but this diagonality condition is not guaranteed to hold in general. Considering instead a fixed-error estimate of the eigenspectrum, Klymko *et al* [9] estimate that the ratio of number of exponential operator applications needed by each algorithm scales asymptotically as

$$\frac{N_{\text{VQPE}}}{N_{\text{QPE}}} \in \tilde{O}\left[\frac{(N_T \sum_j |h_j|)^{9/2} \|S^{-1}\|^{5/2} t_{\max}^{3/2} \min_N |\phi_N^0|^2}{\epsilon}\right] \quad (24)$$

where  $h_j$  are the coefficients of different Pauli terms in the Hamiltonian,  $t_{\max}$  is the maximum step size used in VQPE and  $\epsilon$  is the desired error in the eigenvalues. Which algorithm is more efficient therefore depends significantly on the underlying Hamiltonian and initial state.

### III. CIRCUIT IMPLEMENTATION OF VQPE

In second quantization, a chemistry Hamiltonian may be written as

$$\hat{H} = \sum_{p,q} f_{pq} \hat{a}_p^\dagger \hat{a}_q + \sum_{p,q,r,s} h_{pqrs} \hat{a}_p^\dagger \hat{a}_q^\dagger \hat{a}_r \hat{a}_s, \quad (25)$$

where  $\hat{a}_p^\dagger$  and  $\hat{a}_p$  are fermionic creation and annihilation operators respectively. These operators may be mapped onto strings of Pauli operators acting on qubits by a variety of schemes such as the Jordan-Wigner[21] or Bravyi-Kitaev[22] encodings. For example, in the Jordan-Wigner mapping

$$\hat{a}_j^\dagger = \bigotimes_i^{j-1} Z_i \bigotimes \frac{1}{2}(X_j - iY_j), \quad (26)$$

$$\hat{a}_j = \bigotimes_i^{j-1} Z_i \bigotimes \frac{1}{2}(X_j + iY_j). \quad (27)$$

By applying this transformation to all terms in the Hamiltonian, we obtain the equivalent qubit Hamiltonian

$$\hat{H} = \sum_k \hat{h}_k = \sum_k h_k \hat{P}_k \quad (28)$$

where  $\hat{P}_k$  are strings of Pauli operators. One can then take the first order Trotter-Suzuki approximation to the time evolution operator, for a finite time step of the whole evolution.

$$e^{-i\hat{H}\Delta t} \approx \prod_k e^{-i\hat{h}_k \Delta t} = \hat{U}. \quad (29)$$

This is exact in the limit of an infinitely small time step. Trotterization can be efficiently encoded in a quantum circuit and controlled onto a ancilla, leading to a succession of controlled Pauli gadgets, like those shown in Fig. 2. Propagation by multiple time-steps may then be approximated by

$$e^{-i\hat{H}j\Delta t} \approx \hat{U}^j. \quad (30)$$

We therefore encode  $|\Phi_{j,0}\rangle$  as

$$|\Phi_{j,0}\rangle = \hat{U}^j |\Phi_0\rangle \quad (31)$$

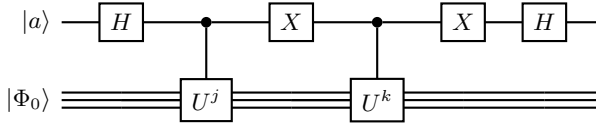


Figure 3. Measurement circuit for  $S_{jk} = \langle \Phi_{j,0} | \Phi_{k,0} \rangle$

where we chose  $|\Phi_0\rangle$  to be the Hartree–Fock wavefunction for the system. In order to compute  $S_{jk}$  we implement the circuit in Fig. 3.

At the end of the circuit, the qubit register is in the state

$$|\Psi\rangle = \frac{1}{2} |0\rangle (|\Phi_{k,0}\rangle + |\Phi_{j,0}\rangle) + \frac{1}{2} |1\rangle (|\Phi_{k,0}\rangle - |\Phi_{j,0}\rangle) \quad (32)$$

and measuring the ancilla in either the  $Z$  or  $Y$  basis gives the real and imaginary parts of  $S_{jk}$  respectively.

$$\begin{aligned} \langle \Psi | Z_a | \Psi \rangle &= \text{Re}(\langle \Phi_{j,0} | \Phi_{k,0} \rangle) \\ \langle \Psi | Y_a | \Psi \rangle &= \text{Im}(\langle \Phi_{j,0} | \Phi_{k,0} \rangle) \end{aligned} \quad (33)$$

Additionally,

$$\begin{aligned} \langle \Psi | Z_a \hat{H} | \Psi \rangle &= \text{Re}(\langle \Phi_{j,0} | \hat{H} | \Phi_{k,0} \rangle) \\ \langle \Psi | Y_a \hat{H} | \Psi \rangle &= \text{Im}(\langle \Phi_{j,0} | \hat{H} | \Phi_{k,0} \rangle) \end{aligned} \quad (34)$$

so Hamiltonian elements may be computed using the same circuit if needed.

In the case of Pauli gadgets, it is easy to implement a controlled gadget, as it only requires controlling the central  $R_z$  gate as can be seen in figure Fig. 2. For number conserving  $\hat{U}$  operators, alternative measurement circuits are possible which do not require controlled operations.[11] We have found that because individual Pauli strings in the trotterized time-evolution operator are not number preserving, these measurement techniques do not perform well in this case. If Eq. (20) holds, we only need to compute the first row elements of the overlap,  $S_{0k}$ , so the circuit in Fig. 3 simplifies to a Hadamard test.

### A. Results

We test this method on  $\text{H}_2$ , linear  $\text{H}_3^+$  and linear  $\text{H}_6$  using the Qiskit Aer shot-based quantum simulator and comparing to results obtained by direct matrix algebra on the corresponding state-vectors. Time-evolved states are constructed by repeating the quantum circuit for unitary  $\hat{U}$  from Eq. (29). The overlap between the initial state  $|\Phi_0\rangle$  and each time-evolved state is obtained by measuring the ancilla in Fig. 3, using 10000 shots in each case. Ten different runs are averaged to obtain the

final results and error bars. In all cases, for the shot-based simulation we consider a threshold of 0.1 on the eigenvalues of the overlap matrix to define the number of linearly independent vectors in the space.

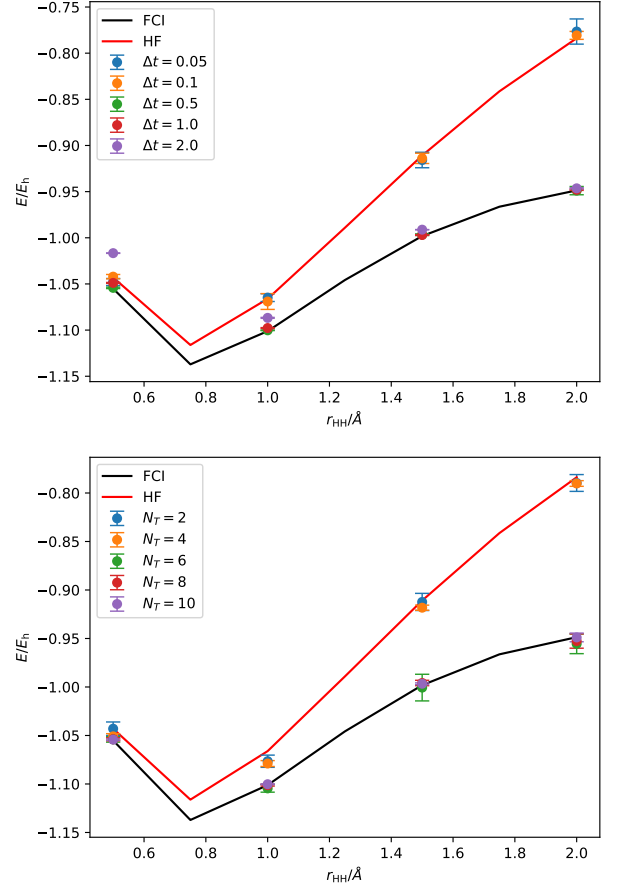


Figure 4.  $\text{H}_2$  binding curve in the STO-3G basis obtained from shot-based VQPE simulations using  $N_T = 10$  and varying sizes of time grid (top) and  $\Delta t = 0.5$  and varying numbers of basis states (bottom).

The Hamiltonian matrix is then diagonalised only in the subset of linearly independent eigenvectors of  $\mathbf{S}$ , with results projected back into the full space of time-evolved states. While lower thresholds could be used for some systems, leading to faster convergence, a large value is more consistent with the high noise we expect from real hardware. For state-vector manipulation, the initial state vector was repeatedly multiplied by the exact matrix corresponding to  $e^{-i\hat{H}\Delta t}$  and a much lower linear dependency threshold ( $10^{-5}$ ) was used.

For  $\text{H}_2$  and  $\text{H}_3^+$  we considered a range of time-steps  $\Delta t \in \{0.05, 0.1, 0.5, 1.0, 2.0\}$  and up to 10 time-steps in each case (see Figs. 4 and 5). For  $\text{H}_6$  we found that the calculations were significantly more sensitive to the size of the time-step, with many values for  $\Delta t$  giving

unphysical energies. Fig. 6 gives results obtained using the best attempted time-steps.

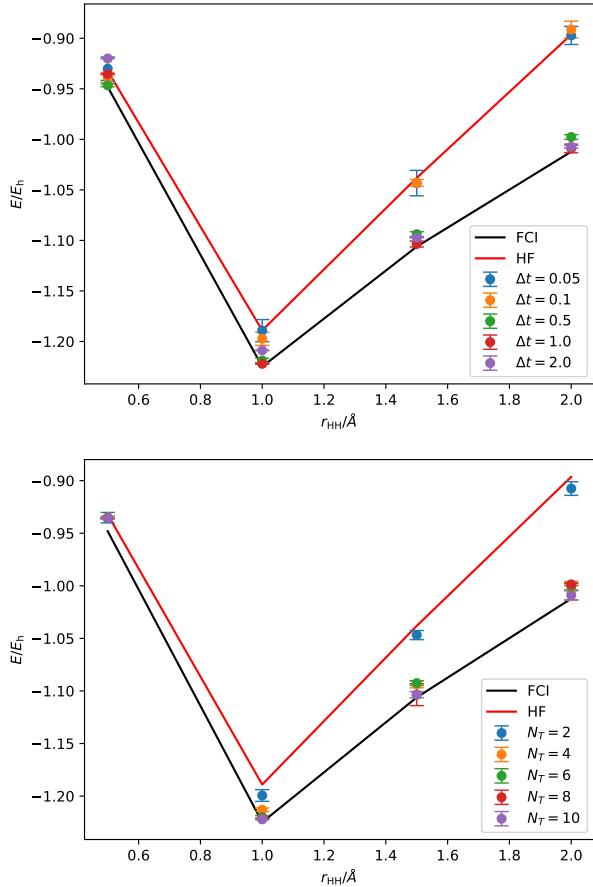


Figure 5. Linear  $\text{H}_3^+$  energy along the symmetric stretching mode in the STO-3G basis obtained from shot-based VQPE simulations using  $N_T = 10$  and varying sizes of time grid (top) and  $\Delta t = 1.0$  and varying numbers of basis states (bottom).

We note a few salient features in these systems. First, convergence with increasing number of time-evolved states is not smooth, but occurs in jumps. For example, in the bottom panel of Fig. 4, we observe that the  $N_T = 2$  and  $N_T = 4$  values oscillate around the HF energy while  $N_T \geq 6$ , the energy is converged to the FCI value.  $\text{H}_6$  shows a similar, multi-stage process, although in this case the energy is not converged by  $N_T = 10$  for stretched geometries (see Fig. 6). Indeed, it is possible for the calculations not to converge at all and merely oscillate around the HF energy if the time-step is too small, as is the case for  $\Delta t = 0.05$  and  $\Delta t = 0.1$  in the  $\text{H}_2$  and  $\text{H}_3^+$  systems.

All of these behaviours can be linked to the variation of the number of linearly independent states in the time-evolved basis. For  $\text{H}_2$ , the eigenbasis is two-

dimensional, so a jump from the HF energy to the FCI is observed when time evolution successfully generates a second linearly independent state. For small  $\Delta t$ , ten steps are not enough to surpass the linear dependency threshold, so no change in energy is observed. If the threshold were lower, the second state may appear after fewer steps, but care needs to be taken to ensure no spurious states are generated by noise. In the noiseless, state-vector simulation of the time-evolution evolving by one time step always generates a linearly independent state and therefore recovers the FCI energy regardless of the size of  $\Delta t$ .

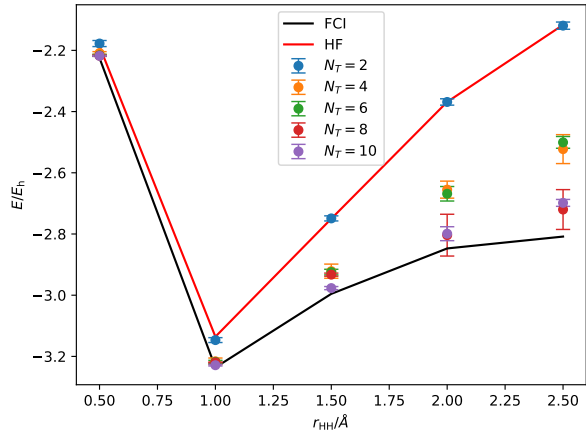


Figure 6.  $\text{H}_6$  chain energy along the symmetric stretch in the STO-3G basis obtained using  $\Delta t = 0.5$  and varying numbers of basis states. At  $r_{\text{HH}} = 0.5$  the results shown are shifted by  $2\pi$  from those directly obtained from the complex logarithm.

Similar behaviour is observed for the  $\text{H}_6$  chain in Fig. 7. At  $\Delta t = 0.5$  and  $r_{\text{HH}} = 2.0$  Å, the simulated state-vector evolution largely introduces one new linearly independent basis state for each time-evolved state, leading to fast, exponential convergence to the full CI solution. The circuit-based evolution introduces independent states much more slowly, with energies agreeing with the state-vector values using the same size of basis.

System	Gates/step	CNOTs/step
$\text{H}_2$	112	34
$\text{H}_3^+$	671	300
$\text{H}_6$	15713	9638

Table I. Number of total gates and CNOTs per trotterised time-evolution step for the  $\text{H}_3^+$  and  $\text{H}_6$  systems in the STO-3G basis set.

Therefore, when using the exact evolution four time-steps are enough to recover the FCI energy, but

significantly more are needed in the circuit-based evolution to get over the increased dependency threshold. This represents a substantial barrier to the application of the VQPE algorithm in this form on NISQ devices.

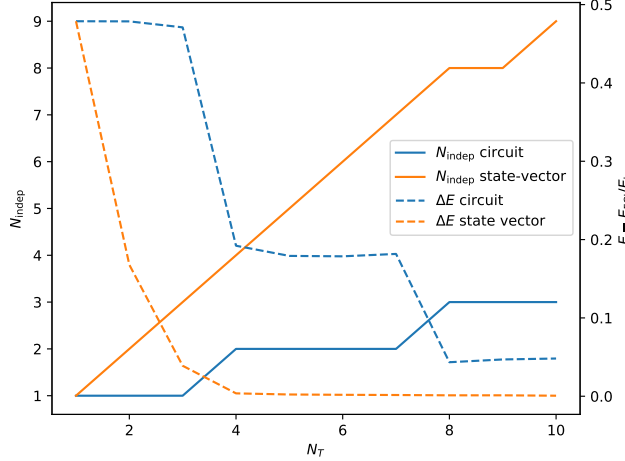


Figure 7. Dependence of the number of linearly independent states (solid lines) and error in the total energy (dashed lines) on the number of time-evolved basis states for the state-vector simulation (orange) and a circuit-based Trotterized time-evolution (blue) of  $H_6$  at  $r_{\text{HH}} = 2.0 \text{ \AA}$ , using  $\Delta t = 0.5$ .

As can be seen from Table I, the number of gates required to evolve the system one step is large and grows rapidly with system size, quickly exceeding the depth of circuit that can be computed within the coherence times of current devices.[23] While in this parametrisation, even one step would be challenging to compute, the number of steps could in principle be reduced by increasing the size of  $\Delta t$  to more quickly surpass the dependency threshold. However, this would have the undesirable side-effect of increasing the error associated with the Trotter decomposition of the time-propagation operator.

#### IV. APPROXIMATING VQPE WITH VARIATIONAL FAST FORWARDING

Faced with the presently intractable increasing depth of time-evolution circuits, we investigate potential routes to circumvent this problem. One approach, which leads to constant depth approximations for time-evolution circuits, is Variational Fast Forwarding (VFF).[16, 17]. In this approach the time-evolution operator is approximated as

$$e^{-i\hat{H}\Delta t} \approx \hat{V}(\boldsymbol{\theta}, \boldsymbol{\gamma}) \approx \hat{W}(\boldsymbol{\theta})\hat{D}(\boldsymbol{\gamma})\hat{W}^\dagger(\boldsymbol{\theta}), \quad (35)$$

where  $\hat{D}$  is a diagonal operator and  $\hat{W}$  is an arbitrary unitary operator. In this case

$$e^{-i\hat{H}\Delta t} \approx \hat{W}\hat{D}^n\hat{W}^\dagger. \quad (36)$$

The diagonal part may be expressed as

$$\hat{D}(\boldsymbol{\gamma}; \Delta t) = \prod_{m=0}^{n-1} \prod_{j \in S_m} e^{i\gamma_j} \otimes_{k=0}^{n-1} (Z_k)^{j_k}, \quad (37)$$

where  $S_m$  is the set of  $n$ -bit binary numbers with  $m$  bits set,  $j_k$  is the value of the  $k^{\text{th}}$  bit in  $j$  and  $\boldsymbol{\gamma}$  is a set of parameters to be variationally optimised. This expression may be further approximated by truncating  $m$ . In this parametrisation,

$$\hat{D}^n(\boldsymbol{\gamma}; \Delta t) = \hat{D}(n\boldsymbol{\gamma}; \Delta t), \quad (38)$$

making the construction of operators for different values of  $\Delta t$  easy and cheap. The  $\hat{W}$  operator can be parametrised in various ways, provided they have enough flexibility to express the required unitary. Different layered ansatze have been used for this[16, 17] and in this work we use the symmetry preserving ansatz,[24] which is number preserving and can also be designed to avoid symmetry and spin contamination. The circuit structure for the controlled evolution operator can be seen in figure Fig. 8.

In order to optimise the parameters  $\boldsymbol{\theta}$  and  $\boldsymbol{\gamma}$  a cost function of the form[17]

$$f(\boldsymbol{\theta}, \boldsymbol{\gamma}) = 1 - \frac{1}{n} \sum_{k=1}^n |\langle \psi | (V^k)^\dagger e^{-iHk\Delta t} | \psi \rangle|^2 \quad (39)$$

is minimized. The cost function is 0 when the overlap between the states generated by time-evolution and those generated by repeatedly applying  $\hat{V}$  is perfect. Exact time-evolution will preserve the support space of the initial wavefunction  $|\psi\rangle$ , so the unitary  $\hat{V}$  must match the action of the time-evolution operator in this space. The No-Free-Lunch theorem [25] then dictates that, in order to fully describe the action of the time-evolution unitary on the support space of the initial state, the cost function would require one term for each dimension in this space.[17] This approach is hardly useful if we are trying to devise a lower-cost alternative to VQPE, as it would require measurements of as many, if not more, overlaps with time-evolved states as the full VQPE approach to obtain and optimise the cost-function, thereby not removing the need for extremely long Trotter circuits.

To overcome this problem, we can relax the condition that the non-orthogonal basis must be constructed from exact time-evolved states. As long as  $\hat{U}$  commutes with the Hamiltonian it will share the same eigenfunctions, giving

$$\hat{U} |\Phi_0\rangle = \sum_N \phi_N^0 \hat{U} |N\rangle = \sum_N \phi_N^0 u_N |N\rangle. \quad (40)$$

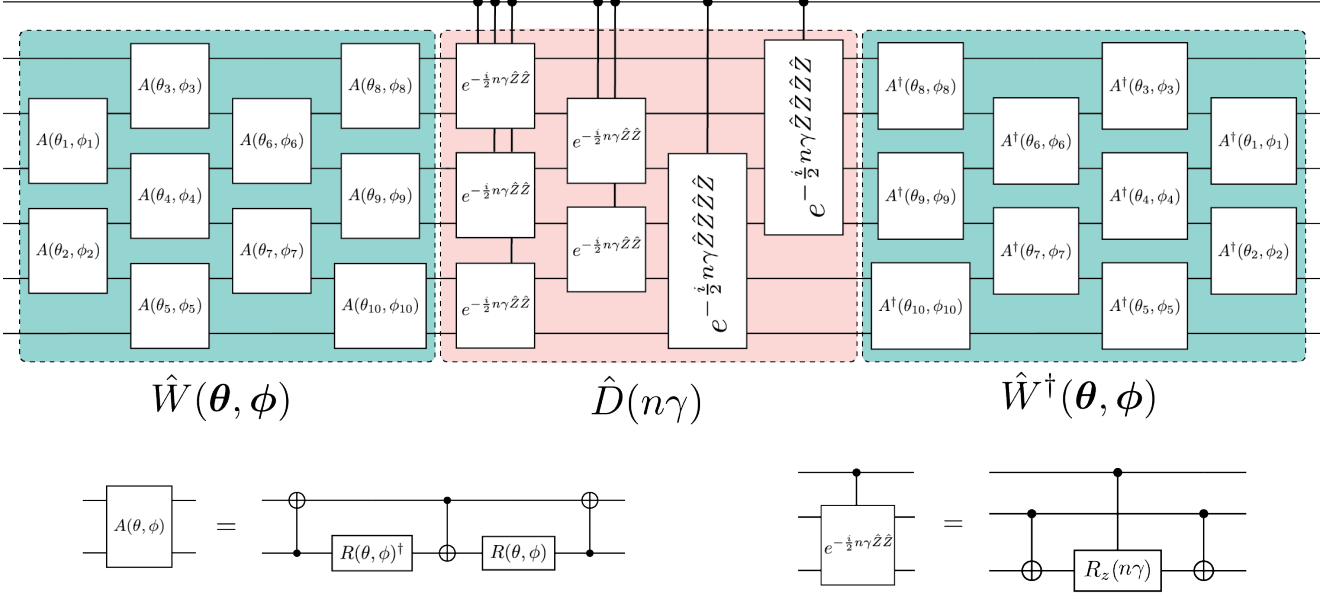


Figure 8. Controlled time evolution operator compiled using variational fast forwarding and number conserving gates. This primitive is used to calculate the overlap  $\langle \Phi_0 | \hat{W} \hat{D}^{k-j} \hat{W}^\dagger | \Phi_0 \rangle$  using the Hadamard test protocol.

The repeated application of  $\hat{U}$  does not change the support space of  $|\Phi_0\rangle$ , so it could be used instead of the time-evolution operator. Unitary operators that do not commute with the Hamiltonian can also be used to generate basis states for exact diagonalisation, however they are not guaranteed to maintain the same support space for all states and therefore may require more basis functions to obtain good estimates of the true eigenstates.

For  $\hat{U} \neq e^{-i\hat{H}\Delta t}$ , there is no longer an explicit relationship between the eigenvalues of the Hamiltonian and those of  $\hat{U}$ , so the former cannot be easily extracted from the diagonalisation of  $\mathbf{U}$ . If  $[\hat{U}, \hat{H}] = 0$ , then the Hamiltonian may be applied to the eigenfunctions of  $\hat{U}$  to obtain the eigenvalues of  $\hat{H}$ . If  $[\hat{U}, \hat{H}] \neq 0$  however, the only option is to construct the Hamiltonian matrix in the basis of states obtained by repeated application of  $\hat{U}$  and directly diagonalise it. We also note that, regardless of the relationship of  $\hat{U}$  with the time-evolution operator, this algorithm amounts to a Krylov subspace diagonalisation, where the space is given by  $\{|\Phi_0\rangle, \hat{U}|\Phi_0\rangle, \hat{U}^2|\Phi_0\rangle, \dots\}$ . Provided enough linearly independent states are considered to span the full support space of this Krylov subspace, the eigenvalues obtained from the diagonalisation should be correct. Therefore we expect that even a poor VFF approximation to  $e^{-i\hat{H}\Delta t}$  could be employed in VQPE and still generate good results, if direct Hamiltonian diagonalisation is used.

## A. Results

We investigate this approach here for  $\text{H}_2$  and 2 electron 2-site Hubbard model, using  $n = 1$  or  $n = 2$  in Eq. (39). Both of these systems have a 6-dimensional Hilbert space, if we take into account both spin projections  $m_s = 0$  and  $m_s = 1$ . While the true time-evolution does not couple these subspaces, we find that the VFF approximation will generate contributions from the  $m_s = 1$  subspace even when starting with an  $m_s = 0$  state. For VFF, we generate the first few exact time-evolved states using a state-vector simulation of the Hamiltonian. We also extract the parameterised state-vector representation of the VFF wave functions from the corresponding circuits and classically compute their overlap and the resulting value of the cost function. Once the VFF parameters are optimised, the overlap and Hamiltonian elements between these states are obtained either from a shot-based simulation with 50000 shots, with linear dependence threshold of 0.1 for the eigenvalues of  $S$ , or from direct matrix algebra on the corresponding state vectors.

Figs. 9 and 10 shows a series of state-vector VFF-based VQPE runs for the 2-site Hubbard model with  $U/t = 0.5$ .

In all cases,  $\hat{D}$  was truncated to  $m = 1$  and  $\hat{W}$  was parametrised by a single-layer symmetry-preserving ansatz, leading to a circuit with a depth of 57 gates, of which 24 are CNOTs. This is a significant improvement from the original trotterised time-evolution, particularly as the depth of this circuit remains constant

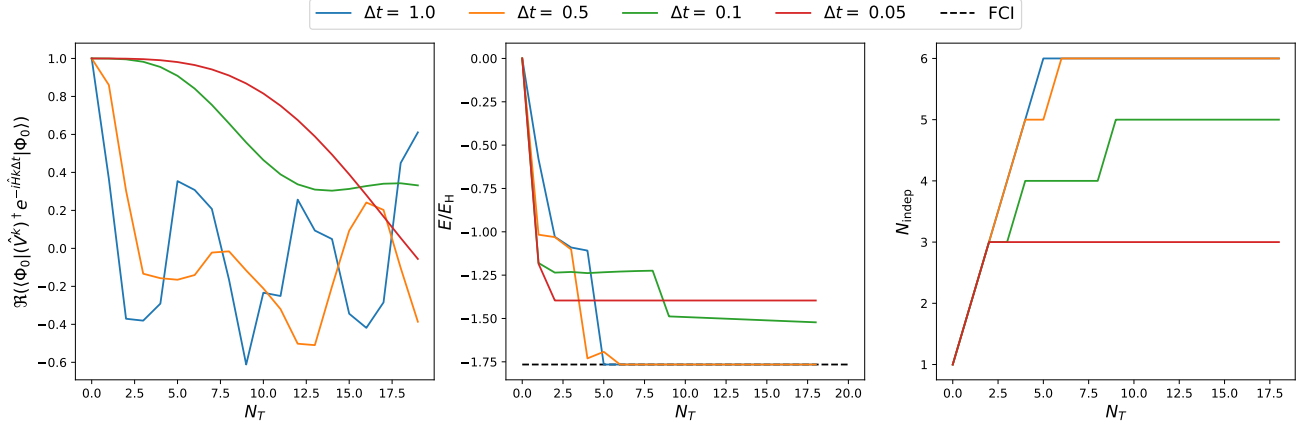


Figure 9. Results obtained by diagonalising the VFF-based VQPE Hamiltonian matrix for the Hubbard dimer with  $U/t = 0.5$ . The VFF circuit was fitted to a single time-step, for  $\Delta t \in \{0.05, 0.1, 0.5, 1.0\}$  and a state-vector quantum circuit simulator was used. The left panel shows the overlap between the  $k$ -th VFF state and the corresponding time-evolved state. The value of the VQPE energy is given in the central panel and the number of linearly independent states is shown in the right panel. The quality of the converged energy is directly linked to the number of independent states in the basis, but shows no clear correlation to the overlap with the true time-evolved states.

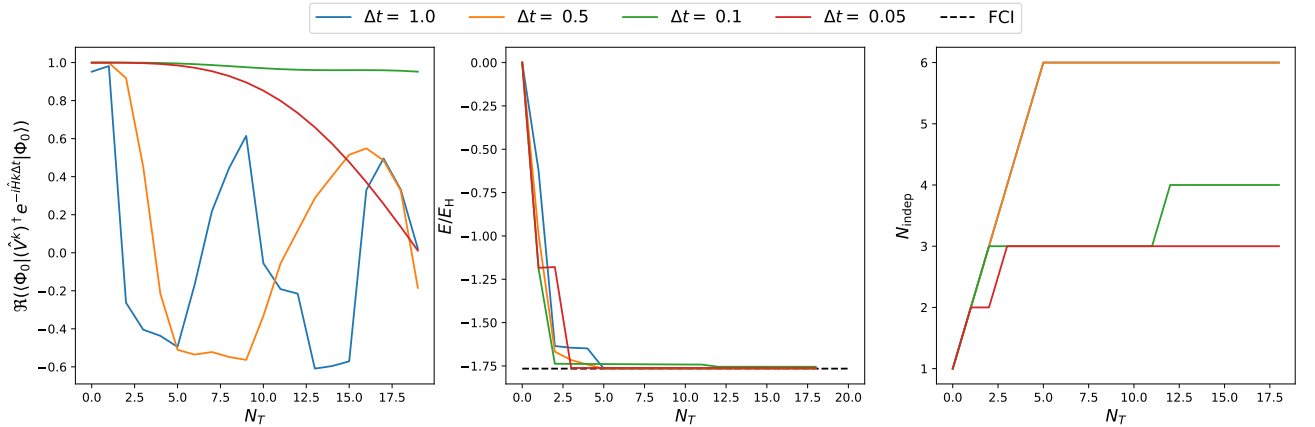


Figure 10. Results obtained by diagonalising the VFF-based VQPE Hamiltonian matrix for the Hubbard dimer with  $U/t = 0.5$ . The VFF circuit was fitted to two time-steps, for  $\Delta t \in \{0.05, 0.1, 0.5, 1.0\}$  and a state-vector quantum circuit simulator was used. The left panel shows the overlap between the  $k$ -th VFF state and the corresponding time-evolved state. The value of the VQPE energy is given in the central panel and the number of linearly independent states is shown in the right panel. In this case we find fast convergence even for calculations that do not span the full Hilbert space, suggesting using a second state in the fitting algorithm mitigates some of the triplet contamination.

for any number of steps. More complex parametrisations were attempted, but no significant change to the results was observed. In the  $n = 1$  case presented in Fig. 9, we find that all methods that successfully generate 6 independent states converge to the true FCI energy, while those that do not fail to recover the true ground state. For  $n = 2$ , all calculations converge to the ground state, even when spanning fewer independent states. This suggests that fitting to more points decreases the contamination from  $m_s = 1$  states. We also note that, as expected from the previous discus-

sion of direct Hamiltonian diagonalisation in the Krylov subspace, the quality of VFF agreement with the true time-evolved states has little correlation with the rate or quality of convergence, with the number of linearly independent states generated being the dominating factor by far.

Fig. 11 shows an equivalent calculation to that in Fig. 10 performed using a shot-based circuit simulation. The behaviour exhibited is qualitatively similar to that of the state-vector simulations, although the effects of random noise are now clearly visible in behaviour such

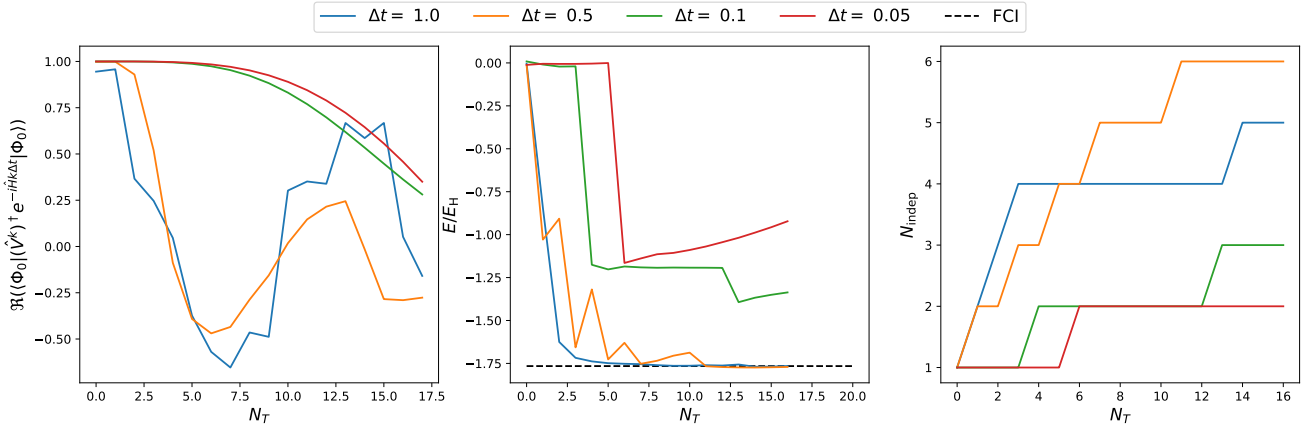


Figure 11. Results obtained by diagonalising the VFF-based VQPE  $\mathbf{U}$  matrix for the Hubbard dimer with  $U/t = 0.5$ . The VFF circuit was fitted to two time-steps, for  $\Delta t \in \{0.05, 0.1, 0.5, 1.0\}$  and a shot-based quantum circuit simulator was used. The left panel shows the overlap between the  $k$ -th VFF state and the corresponding time-evolved state. The value of the VQPE energy is given in the central panel and the number of linearly independent states is shown in the right panel. Convergence is similar to state-vector simulations, but the presence of stochastic noise introduces noticeable kinks in the overlap and energy curves.

as the unphysical upwards drift in the  $\Delta t = 0.05$  energy. Nevertheless, larger time-steps lead to successful convergence to the ground state.

$\min \left( \text{Re} \left\{ \langle \psi   (V^k)^\dagger e^{-i \hat{H} k \Delta t}   \psi \rangle \right\} \right)   E_{\text{VQPE}} - E_{\text{FCI}}$	
0.844	0.1639
0.852	0.1128
0.95570	-0.0409
0.95744	-0.0426
0.95748	0.0131

Table II. Error in the VQPE energy for the Hubbard dimer obtained by diagonalising the  $\mathbf{U}$  matrix as a function of minimum overlap between the VFF and time-evolved states. We find the error to decrease as agreement between the two increases.

One of the significant advantages of VQPE is that, in the basis of time-evolved states, the overlap matrix  $\mathbf{S}$  can be computed with linear cost due to Eq. (20). This remains rigorously the case for VFF approximate states, for which

$$\begin{aligned}
 S_{jk} &= \langle \Phi_0 | \hat{W} \hat{D}^{-j} \hat{W}^\dagger \hat{W} \hat{D}^k \hat{W}^\dagger | \Phi_0 \rangle \\
 &= \langle \Phi_0 | \hat{W} \hat{D}^{-j} \hat{D}^k \hat{W}^\dagger | \Phi_0 \rangle \\
 &= \langle \Phi_0 | \hat{W} \hat{D}^{k-j} \hat{W}^\dagger | \Phi_0 \rangle \\
 &= S_{j+n, k+n}, \forall n \in \mathbb{Z}
 \end{aligned} \tag{41}$$

Hamiltonian diagonalisation is resilient to a poor VFF approximation as its quality depends only on a basis sets ability to span the relevant support space.. That is not the case for Eq. (16) with  $\mathbf{U}$  defined as in Eq. (19).

If the VFF states are poor approximations to the true time-evolved states,

$$U_{jk} = S_{j,k+1} \neq \langle \Phi_j | e^{-i \hat{H} \Delta t} | \Phi_k \rangle, \tag{42}$$

the eigenvalues of  $\mathbf{U}$  are no longer clearly related to the Hamiltonian eigenvalues. However, if the approximation is good enough, it should be possible to employ this approach. We consider the  $\Delta t = 0.1$  case for the Hubbard model in Fig. 10 and attempt to construct the  $\mathbf{U}$  matrix from the overlap. Table II gives the results of the diagonalisations of a series of such matrices.

We find that on a large scale the resulting energy converges with improved overlap with the true energy, while close to perfect agreement it oscillates about the true FCI value. As can be seen from Figs. 4 to 6, some oscillation is also present in the shot-based results based on the true time-evolved states. These results are promising and suggest that, given a reliably good Hamiltonian approximation, the VFF-based VQPE method can also be applied with only linear cost in the number of basis functions used. Further exploration into how to guarantee the quality of the approximation is warranted.

Finally, we return our attention to  $\text{H}_2$ . While general physical hamiltonians cannot necessarily be fast forwarded,[16, 26] we find that in this case it is possible to obtain a good VFF approximation to the time-evolution. Results obtained with VFF and VQPE are given in Fig. 12. We also find that in most cases the error in the overlap with the true trotterised state is less than  $10^{-6}$ , so this system can be well treated with the unitary approach, as can be seen in Fig. 13.

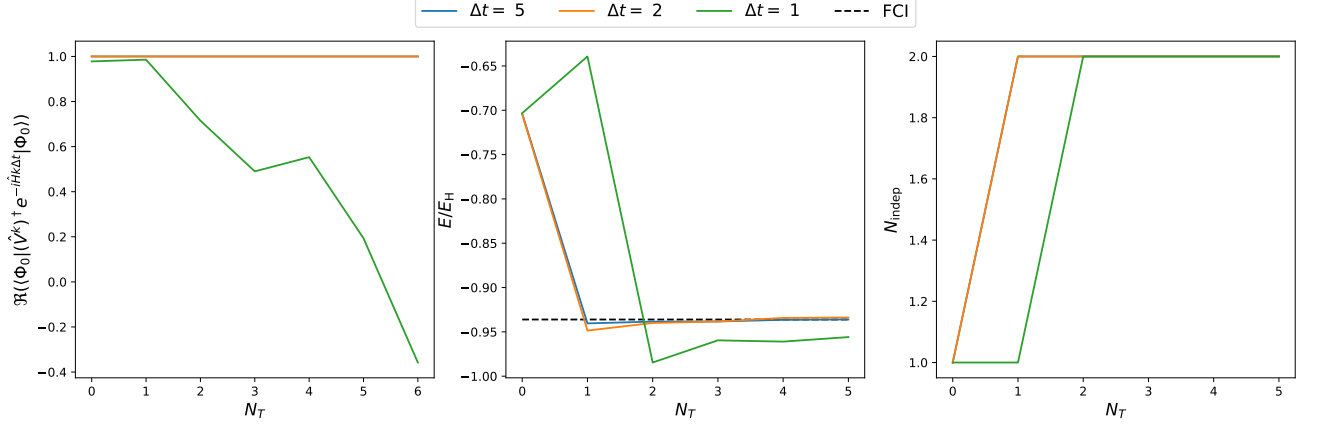


Figure 12. Results obtained by diagonalisation of the VFF-based VQPE Hamiltonian matrix for  $\text{H}_2$  at  $r_{\text{HH}} = 2.5\text{\AA}$ . The VFF circuit was fitted to two time-steps, for  $\Delta t \in \{1, 2, 5\}$  and a shot-based quantum circuit simulator was used. The left panel shows the overlap between the  $k$ -th VFF state and the corresponding time-evolved state. The value of the VQPE energy is given in the central panel and the number of linearly independent states is shown in the right panel. In this case, we observe a correlation between the quality of the overlap between the fast-forwarded state and the true time-evolved state, and the rate of convergence of VQPE.

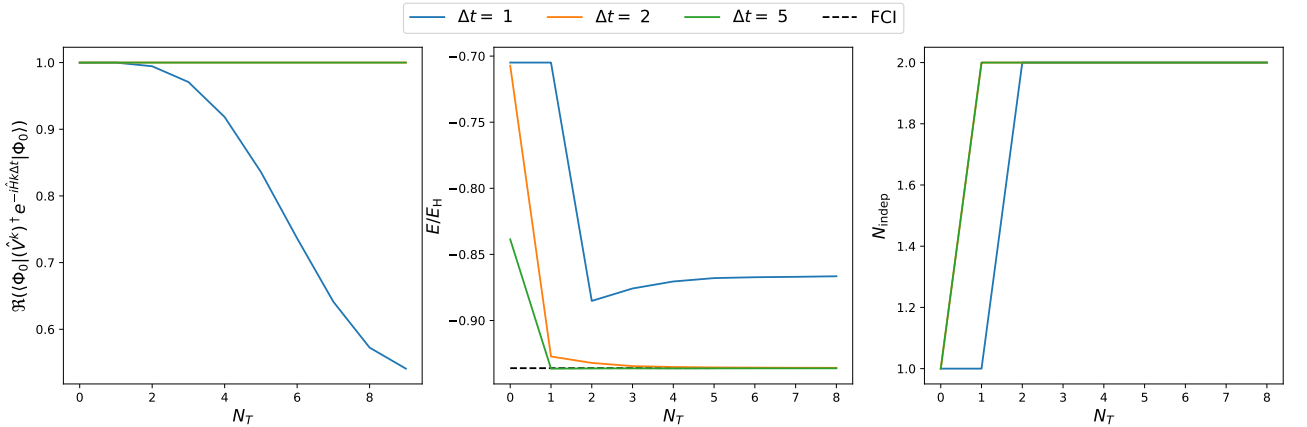


Figure 13. Results obtained by diagonalisation of the VFF-based VQPE  $\mathbf{U}$  matrix for  $\text{H}_2$  at  $r_{\text{HH}} = 2.5\text{\AA}$ . The VFF circuit was fitted to two time-steps, for  $\Delta t \in \{1, 2, 5\}$  and a shot-based quantum circuit simulator was used. The left panel shows the overlap between the  $k$ -th VFF state and the corresponding time-evolved state. The value of the VQPE energy is given in the central panel and the number of linearly independent states is shown in the right panel.

A binding curve for the system is also given in Fig. 14, with energies consistently within one standard deviation of the FCI value. Somewhat surprisingly, results obtained from the diagonalisation of the  $\mathbf{U}$  matrix have smaller error bars than those obtained from the Hamiltonian. This may be due to the fact that the  $\mathbf{U}$  and  $\mathbf{S}$  matrices are obtained from the same set of measurements, leading to correlated errors in the two which may cancel in the overall result.

## V. CONCLUSIONS

We have presented a circuit-based implementation for the VQPE algorithm based on Trotterized time propagation and the Hadamard test. This algorithm was implemented successfully on both state-vector and shot-based quantum simulators and we find that the method is successful in finding the ground state of the  $\text{H}_2$  and  $\text{H}_3^+$  systems, but requires a prohibitively large number of one- and two-qubit gates to converge for  $\text{H}_6$ . This is an inevitable consequence of Trotterized time-evolution and would prevent this algorithm from finding significant

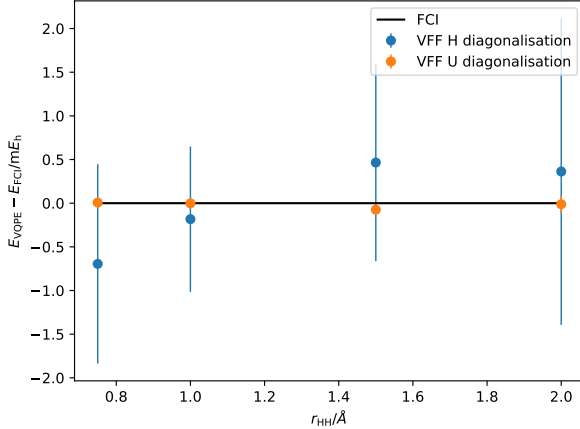


Figure 14. VFF-based VQPE binding curve for  $\text{H}_2$  in the STO-3G basis set. In all cases the VFF circuit was fitted to two time-steps using  $\Delta t = 5$  and a shot-based quantum simulator was employed to measure the resulting matrices. Results given are obtained from the diagonalisation of the matrices after 10 time-steps, all of which include two linearly-independent states

use of NISQ devices.

We propose an approximation to the VQPE algorithm using the VFF approach, which reduced the circuit depth of the time-evolution circuits to roughly that of a single Trotter step. The approximation provides a sensible Krylov subspace basis for Hamiltonian diagonalisation even when its fidelity to the true time-evolved basis is low. We find our particular choice of VFF decomposition natively preserves electron number but not  $m_s$  values, unlike true time-evolution, so potentially requires more linearly independent states to reach the true ground state. This contamination can be reduced by using more time-evolved states in the cost function for VFF optimisation.

In general, VQPE based on VFF states requires construction of the Hamiltonian matrix, so a quadratic number of calls to the quantum processor. However, where  $\langle \psi | (V^k)^\dagger e^{-iHk\Delta t} | \psi \rangle$  is close to unity across the entire range of VFF states considered, diagonalising the matrix  $\mathbf{U}$  defined in Eq. (19) gives a good approximation of the true Hamiltonian eigenstates. In this case, VFF can be used to reduced required quantum circuit depth while maintaining the linear cost of matrix generation of exact VQPE.

---

[1] J. Preskill, *Quantum* **2**, 79 (2018).

[2] A. Peruzzo, J. McClean, P. Shadbolt, M.-H. Yung, X.-Q. Zhou, P. J. Love, A. Aspuru-Guzik, and J. L. O’Brien, *Nat. Commun.* **5**, 4213 (2014).

[3] P. J. J. O’Malley, R. Babbush, I. D. Kivlichan, J. Romero, J. R. McClean, R. Barends, J. Kelly, P. Roushan, A. Tranter, N. Ding, B. Campbell, Y. Chen, Z. Chen, B. Chiaro, A. Dunsworth, A. G. Fowler, E. Jeffrey, E. Lucero, A. Megrant, J. Y. Mutus, M. Neeley, C. Neill, C. Quintana, D. Sank, A. Vainsencher, J. Wenner, T. C. White, P. V. Coveney, P. J. Love, H. Neven, A. Aspuru-Guzik, and J. M. Martinis, *Phys. Rev. X* **6**, 031007 (2016).

[4] C. Hempel, C. Maier, J. Romero, J. McClean, T. Monz, H. Shen, P. Jurcevic, B. P. Lanyon, P. Love, R. Babbush, A. Aspuru-Guzik, R. Blatt, and C. F. Roos, *Phys. Rev. X* **8**, 031022 (2018).

[5] S. McArdle, T. Jones, S. Endo, Y. Li, S. C. Benjamin, and X. Yuan, *npj Quantum Info.* **5**, 75 (2019).

[6] R. M. Parrish and P. L. McMahon, “Quantum filter diagonalization: Quantum eigendecomposition without full quantum phase estimation,” (2019), [arXiv:1909.08925 \[quant-ph\]](https://arxiv.org/abs/1909.08925).

[7] A. Y. Kitaev, “Quantum measurements and the abelian stabilizer problem,” (1995), [arXiv:quant-ph/9511026](https://arxiv.org/abs/quant-ph/9511026).

[8] A. Aspuru-Guzik, A. D. Dutoi, P. J. Love, and M. Head-Gordon, *Science* **309**, 1704 (2005).

[9] K. Klymko, C. Mejuto-Zaera, S. J. Cotton, F. Wudarski, M. Urbanek, D. Hait, M. Head-Gordon, K. B. Whaley, J. Moussa, N. Wiebe, W. A. de Jong, and N. M. Tubman, *PRX Quantum* **3**, 020323 (2022).

[10] J. R. McClean, M. E. Kimchi-Schwartz, J. Carter, and W. A. de Jong, *Phys. Rev. A* **95**, 042308 (2017).

[11] W. J. Huggins, J. Lee, U. Baek, B. O’Gorman, and K. B. Whaley, *New J. Phys.* **22** (2020), 10.1088/1367-2630/ab867b, [arXiv:1909.09114](https://arxiv.org/abs/1909.09114).

[12] M. Motta, C. Sun, A. T. K. Tan, M. J. O’Rourke, E. Ye, A. J. Minnich, F. G. S. L. Brandão, and G. K.-L. Chan, *Nat. Phys.* **16**, 231 (2020).

[13] N. H. Stair, R. Huang, and F. A. Evangelista, *Journal of Chemical Theory and Computation* **16**, 2236 (2020), PMID: 32091895, <https://doi.org/10.1021/acs.jctc.9b01125>.

[14] C. L. Cortes and S. K. Gray, *Phys. Rev. A* **105**, 022417 (2022).

[15] G. Golub and C. Van Loan, *Matrix Computations*, The North Oxford Academic paperback (North Oxford Academic, 1983).

[16] C. Cîrstoiu, Z. Holmes, J. Iosue, L. Cincio, P. J. Coles, and A. Sornborger, *npj Quantum Inf.* **6**, 82 (2020).

[17] J. Gibbs, K. Gili, Z. Holmes, B. Commeau, A. Ar rasmith, L. Cincio, P. J. Coles, and A. Sornborger, “Long-time simulations with high fidelity on quantum hardware,” (2021), [arXiv:2102.04313 \[quant-ph\]](https://arxiv.org/abs/2102.04313).

[18] E. Farhi, J. Goldstone, S. Gutmann, and M. Sipser, “Quantum computation by adiabatic evolution,” (2000), [arXiv:quant-ph/0001106](https://arxiv.org/abs/quant-ph/0001106).

[19] E. Farhi, J. Goldstone, S. Gutmann, J. Lapan, A. Lundgren, and D. Preda, *Science* **292**, 472 (2001), <https://www.science.org/doi/pdf/10.1126/science.1057726>.

[20] A. Krylov, *Bull. Acad. Sci. URSS* **1931**, 491 (1931).

[21] P. Jordan and E. Wigner, *Z. Phys.* **47**, 631 (1928).

- [22] S. B. Bravyi and A. Y. Kitaev, *Ann. Phys.* **298**, 210 (2002).
- [23] N. M. Linke, D. Maslov, M. Roetteler, S. Debnath, C. Figgatt, K. A. Landsman, K. Wright, and C. Monroe, *PNAS* **114**, 3305 (2017), <https://www.pnas.org/content/114/13/3305.full.pdf>.
- [24] B. T. Gard, L. Zhu, G. S. Barron, N. J. Mayhall, S. E. Economou, and E. Barnes, *npj Quantum Inf.* **6**, 10 (2020).
- [25] K. Poland, K. Beer, and T. J. Osborne, “No free lunch for quantum machine learning,” (2020).
- [26] Y. Atia and D. Aharonov, *Nat. Commun.* **8**, 1572 (2017).